Mathematics

Research article

Entropy formation analysis for magnetized UCM fluid over an exponentially stretching surface with PST and PSHF wall conditions

Sheheryar Shah[1], M. N. Abrar[2], Kamran Akhtar [3], Aziz Khan [4] and Thabet Abdeljawad [4,5,6,*]

[1] School of Mathematics and Statistics, Xi'an Jiaotong University, Xi'an, Shaanxi 710049, China
[2] Department of Civil Engineering, National University of Sciences and Technology, Balochistan Campus, Quetta, Pakistan
[3] National University of Sciences and Technology (NUST), Islamabad, Pakistan
[4] Department of Mathematics and Sciences, Prince Sultan University, Riyadh 11586, Saudi Arabia
[5] Department of Medical Research, China Medical University, Taichung 40402, Taiwan
[6] Department of Mathematics, Kyung Hee University, 26 Kyungheedae-ro, Dongdaemun-gu, Seoul 02447, Republic of Korea

* Correspondence: Email: tabdeljawad@psu.edu.sa.

Abstract: This article aims to demonstrate the formation of entropy due to variable thermal conductivity, radiation, and fluid friction irreversibilies for a three-dimensional upper-convected Maxwell (UCM) fluid. The fluid motion occurs as a result of exponential stretching sheets. Separate discussions are held regarding the entropy generation related to the prescribed surface temperature and prescribed surface heat flux. Additionally, the heat transport mechanism is examined in the presence of thermal radiation. The governing physical situation is first modeled and then solved by using the homotopy analysis method to acquire the solution. The physical importance of relevant flow parameters is shown graphically and in tabular form. It is noted that the entropy generated is reduced with an increase in the thermal radiation parameter. Streamline patterns are also drawn for two- and three-dimensional UCM fluid models. Finally, the current analytical solution is found to be in agreement with the solutions in the literature.

Mathematics Subject Classification: 65L10, 76A05, 76D05, 76W05

Abbreviations: α : Stretching ratio; λ : Relaxation time; *L*: Reference length; *Pr*: Prandtl number; Re : Reynolds number; β: Deborah number; *v*: Kinematic viscosity; Br : Brinkman number; Ψ : Viscous dissipation; μ: Dynamic viscosity; *k*: Thermal conductivity; *Rn*: Radiation parameter; $\sigma*$: Stefan-Boltzmann constant; *A, B*: Temperature exponents; E_G : Entropy generation number; $k*$: Mean absorption coefficient; ξ : Finite temperature difference; c_p: Specific heat at constant pressure; θ: Dimensionless temperature in PST; ϕ : Dimensionless temperature in PSHF; γ Temperature-dependent thermal conductivity

1. Introduction

The primary issue that is emerging in any industry these days is the effective transport of energy. In this modern era of science and technology, almost all mechanical machines that work with thermo-fluidic systems face this energy loss. Basically, all thermo-fluidic structures bring in irreversibilities, resulting in an energy drop. This loss of thermal energy reduces the system's capacity for thermal competence. In 1850, the German physicist Rudolf Clausius initially introduced his theory of this energy/efficiency loss as "entropy." Clausius' concept of entropy was like a candle in a dark room for the scientists of the 19th century. The second law mechanism is a splendid and productive guideline to figure out the entropy of any engineering machine. Actually, entropy is linked to several energy-related fields, including geothermal power generation, the cooling of cutting-edge electronics, and solar energy generation. Initially, Bejan [1] presented entropy as a philosophical concept. Bejan analyzed the effects of heat transfer and viscous dissipation on entropy formation. Rashidi et al. [2] investigated the entropy production that occurs due to fluid friction and the irreversibility of Joule dissipation when it passes through a porous duct. Aksoy [3] studied entropy formation due to fully developed flow in a rectangular porous duct. In their paper, Abrar et al. [4] explore the entropy production that occurs as a result of heat transport, viscosity, and magnetic irreversibility. Kamran et al. [5] numerically studied the entropy formation of Casson fluid flow over a slip boundary. Rashid and Mustafa's [6] study focused on the flow of a Reiner-Rivlin fluid across a stretchable, rotating surface, as well as its effects on viscous heating. Recently, Abrar et al. [7−11] conducted many studies related to entropy with multiple physical constraints of interest.

There have been remarkable advancements in scientific research and technological development due to an approach known as boundary layer flow over moving surfaces with heat transfer. Various applications, such as crystal growth, glass fiber production, paper-making, continuous casting, metallurgical operations, the cooling of metallic sheets in cooling baths, and plastic film design, have benefited from this approach. The pioneering study on stretching surfaces was initially proposed by Sakiadis [12]. After this fundamental approach, many researchers have contributed to demonstrating two-dimensional flows over a stretching surface with different aspects due to their demanding applications. However, three-dimensional flows for such cases have not been extensively examined yet due to their complex mathematical nature. A few recent studies for three-dimensional flows via different

flow assumptions include the following: Singh [13] analytically solved the double-diffusive boundary layer analysis for Newtonian fluids, Razzaq et al. [14] presented the flow of a magnetized nanofluid over a stretching plate by using a non-similar approach, Razzaq and Farooq [15] investigated convection analysis for the Oldroyd-B model past a stretching surface, Cui et al. [16] studied the consequences of magnetic dissipation, viscous dissipation, and chemical reaction in the flow, temperature, and concentration fields, Umer et al. [17] and Farooq et al. [18] separately discussed computational analyses for forced and mixed convection, and Talat et al. [19] explored the flow over a rotating porous disk. Qaiser et al. [20] numerically addressed the mixed convection flow of a nanofluid across a stretched surface, Khan et al. [21] explored the properties of a Maxwell bio-nanofluid in the presence of solar radiation, Cui et al. [22−24] discussed heat transport analysis in a biconvection model with different body forces, Khan et al. [25] discussed the Marangoni convection flow due to a rotating disk, Guo et al. [26] examined entropy analysis for a radiative nanofluid, Ali et al. [27,28] examined heat and mass transport for three-dimensional nanofluids over a stretching sheet, Khattak et al. [29] numerically examined the heat flux model past a nonlinear stretching surface, and Khan et al. [30] analyzed the entropy generation for micro-rotating Casson fluid flow.

Motivated by the above-cited literature review, this study was purposed to examine the entropy formation due to temperature-dependent thermal conductivity for a three-dimensional flow of a Maxwell fluid past an exponentially stretching sheet. Furthermore, a heat transport investigation was performed under two different heat circumstances, i.e., a prescribed surface temperature (PST) and prescribed surface heat flux (PSHF). Series solutions were produced for velocity and temperature profiles by using a semi-analytical approach called the homotopy analysis method (HAM). In the forthcoming section, the authors disclose the problem formulation. Section 3 formulates the formula for the entropy formation in the presence of a PST and PSHF. In Section 4, the authors address the series solution of the governed mathematical model. Section 5 presents to present the physical importance of the governed model through plots and tables. The last section reflects the concluding remarks of the study.

2. Problem formulation

In this study, consideration has been given to the three-dimensional flow of a Maxwell fluid bounded past an exponentially stretching sheet. Using the Cartesian coordinate system, x and y axes were selected to be parallel to the direction of motion along the sheet, whereas the z- axis was chosen to be perpendicular to the axis of motion. The driving force for the fluid is the stretching sheet at $z = 0$, U_w and V_w represents the fluid stretching velocities in the x and y directions, respectively. Figure 1 reflects the systematic view of the physical model.
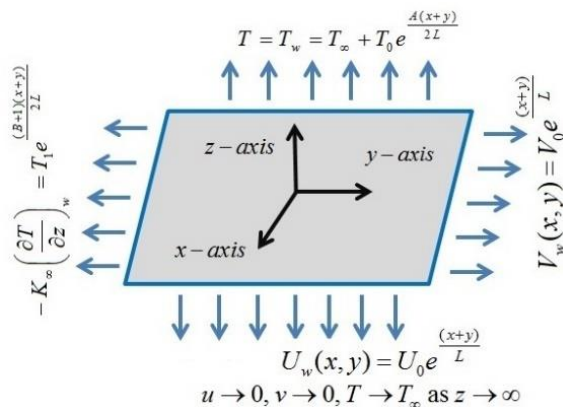
Figure 1. Position and orientation.

The flow is governed by the following relations:

$$\frac{\partial u}{\partial x} + \frac{\partial v}{\partial y} + \frac{\partial w}{\partial z} = 0, \tag{1}$$

$$u\frac{\partial u}{\partial x} + v\frac{\partial u}{\partial y} + w\frac{\partial u}{\partial z} = v\frac{\partial^2 u}{\partial z^2} - \lambda\left(u^2\frac{\partial^2 u}{\partial x^2} + v^2\frac{\partial^2 u}{\partial y^2} + w^2\frac{\partial^2 u}{\partial z^2}\right) + 2\lambda\left(uv\frac{\partial u^2}{\partial x\partial y} + vw\frac{\partial u^2}{\partial y\partial z} + uw\frac{\partial u^2}{\partial x\partial z}\right), \tag{2}$$

$$u\frac{\partial v}{\partial x} + v\frac{\partial v}{\partial y} + w\frac{\partial v}{\partial z} = v\frac{\partial^2 u}{\partial z^2} - \lambda\left(u^2\frac{\partial^2 v}{\partial x^2} + v^2\frac{\partial^2 v}{\partial y^2} + w^2\frac{\partial^2 v}{\partial z^2}\right) + 2\lambda\left(uv\frac{\partial^2 v}{\partial x\partial y} + vw\frac{\partial^2 v}{\partial y\partial z} + uw\frac{\partial^2 v}{\partial x\partial z}\right), \tag{3}$$

and the supported boundary conditions for the assumed physical situation are as follows:

$$u = U_w, \quad v = V_w, \quad w = 0, \quad at \quad z = 0 \; and \; u \to 0, \quad v \to 0, \quad as \quad z \to \infty; \tag{4}$$

Let us introduce the convenient variables:

$$\eta = \sqrt{\frac{U_0}{2Lv}}e^{\frac{x+y}{2L}}z, u = U_0 e^{\frac{x+y}{L}}f'(\eta), \; v = U_0 e^{\frac{x+y}{L}}g'(\eta)$$

$$w = -\sqrt{\frac{vU_0}{2L}}e^{\frac{x+y}{2L}}\big(f(\eta) + g(\eta) + \eta(f'(\eta) + g'(\eta))\big). \tag{5}$$

As a result, (2) and (3) simplify to (1), and (1) is satisfied automatically.

$$f''' - 2(f' + g')f' + (f + g)f'' - \beta\left(2(f' + g')^2 f' - \frac{\eta}{2}(f' + g')^2 f''\right)$$

$$-\beta\left(\frac{1}{2}(f + g)^2 f''' - 3f(f' + g')f'' - 3g(f' + g')f''\right) = 0, \tag{6}$$

$$g''' - 2(f' + g')g' + (f + g)g'' - \beta\left(2(f' + g')^2 g' - \frac{\eta}{2}(f' + g')^2 g''\right)$$

$$-\beta \left(\frac{1}{2}(f+g)^2 g''' - 3f(f'+g')g'' - 3g(f'+g')g'' \right) = 0, \tag{7}$$

where the appropriate boundary conditions are as follows:

$$f = 0, \quad f' = 1, \quad g = 0, \quad g' = \alpha, \quad at \quad \eta = 0 \; and$$

$$f' \to 0, \quad g' \to 0, \quad as \quad \eta \to \infty; \tag{8}$$

here $\beta = \frac{\lambda U_m}{2L}$ represents the Deborah number, where U_m is of $O\left(U_0 e^{x+y/L}\right)$ and $\alpha = \left(\frac{V_0}{U_0}\right)$ represents the stretching ratio parameter. Note that, for $\alpha = 0$, the three-dimensional flow becomes two-dimensional flow (i.e., $g = 0$) which is:

$$f''' - 2f'^2 + ff'' - \beta \left(2f'^3 - \frac{\eta}{2}f''f'^2 + \frac{1}{2}f^2 f''' - 3ff'f'' \right) = 0, \tag{9}$$

$$f = 0, \quad f' = 1, \quad as \quad \eta = 0 \; and \; f' \to 0 \quad as \quad \eta \to \infty; \tag{10}$$

also, when we set $\alpha = 1$, one can reach the axisymmetric flow (i.e., $f = g$) with similar boundary conditions as (10).

2.1. Heat transfer mechanism

The heat transport equation with the thermal radiation phenomenon has the following form:

$$u\frac{\partial T}{\partial x} + v\frac{\partial T}{\partial y} + w\frac{\partial T}{\partial z} = \frac{1}{\rho c_p}\frac{\partial}{\partial z}\left(\left(k(T) + \frac{16T_\infty^3 \sigma*}{3k*} \right)\frac{\partial T}{\partial z} \right), \tag{11}$$

and the wall conditions for the PST and PSHF circumstances are as follows:

$$T = T_w = T_\infty + T_0 e^{\frac{A(x+y)}{2L}} \quad at \quad z = 0 \; and \; T \to T_\infty \quad as \quad z \to \infty,$$

$$-k_\infty \left(\frac{\partial T}{\partial z}\right)_w = T_1 e^{\frac{(B+1)(x+y)}{2L}} \quad at \quad z = 0 \; and \; T \to T_\infty \quad as \quad z \to \infty. \tag{12}$$

It may be shown that the thermal conductivity (k) is a function of temperature in the following way:
PST case:

$$k = k_\infty \big(1 + \gamma.\theta(\eta)\big);$$

PSHF case:

$$k = k_\infty \big(1 + \gamma.\varphi(\eta)\big); \tag{13}$$

a similarity transformation is introduced as

$$T = T_\infty + T_0 e^{\frac{A(x+y)}{2L}} \theta(\eta) \quad and \; T = T_\infty + \frac{T_1}{k_\infty}\sqrt{\frac{2vL}{U_0}} e^{\frac{B(x+y)}{2L}} \varphi(\eta) . \tag{14}$$

Equation (11) reduces to the following forms after using (14):

$$(1 + Rn + \gamma\theta)\theta'' + Pr(f + g)\theta' - A.Pr(f' + g')\theta + \gamma\theta'^2 = 0, \tag{15}$$

$$(1 + Rn + \gamma\varphi)\varphi'' + Pr(f + g)\varphi' - B.Pr(f' + g')\varphi + \gamma\varphi'^2 = 0; \tag{16}$$

The reduced boundary conditions are as follows:

$$\theta = 1, \quad \varphi' = -\frac{1}{1+\gamma}, \quad at \quad \eta = 0, and \; \theta \to 0, \quad \varphi \to 0, \quad at \quad \eta \to \infty, \tag{17}$$

where the Prandtl number and the radiation parameter are given as $\left(Pr = {\mu c_p}/{k_\infty}\right)$ and $\Big(Rn = {16\sigma * T_\infty{}^3}/{3k_\infty k *}\Big)$ respectively.

3. Second law analysis with a PST and PSHF

The philosophy of the second law of thermodynamics offers a computational way by which one can compute the irreversibilities in any system. The volumetric entropy generation rate $\left(S_{Gen}\right)$ and viscous dissipation $\left(\Psi\right)$ are a result of the following calculations [10]:

$$S_{Gen} = \frac{k(T)}{T_\infty^2}\left\{\left(\frac{\partial T}{\partial x}\right)^2 + \left(\frac{\partial T}{\partial y}\right)^2 + \left(\frac{\partial T}{\partial z}\right)^2\right\} + \frac{16T_\infty{}^3\sigma*}{3k*}\left\{\left(\frac{\partial T}{\partial x}\right)^2 + \left(\frac{\partial T}{\partial y}\right)^2 + \left(\frac{\partial T}{\partial z}\right)^2\right\} + \frac{\mu}{T_\infty}\Psi, \tag{18}$$

$$\Psi = \left\{2\left[\left(\frac{\partial u}{\partial x}\right)^2 + \left(\frac{\partial v}{\partial y}\right)^2 + \left(\frac{\partial w}{\partial z}\right)^2\right] + \left(\frac{\partial u}{\partial y} + \frac{\partial v}{\partial x}\right)^2 + \left(\frac{\partial u}{\partial z} + \frac{\partial w}{\partial x}\right)^2 + \left(\frac{\partial v}{\partial z} + \frac{\partial w}{\partial y}\right)^2\right\}, \tag{19}$$

where $\left(S_{gen}\right)$ is the rate at which characteristic entropy is generated

$$S_{gen} = \frac{k_\infty}{T_\infty^2}\left(\frac{\Delta T}{L}\right)^2. \tag{20}$$

3.1. Incorporating the PST

The dimensionless local generation entropy (E_G) is defined in the following way:

$$E_G = \frac{S_{Gen}}{S_{gen}} = \underbrace{\frac{(1+\gamma\theta)}{2}\{(A\theta + \eta\theta')^2 + Re\,\theta'^2\}}_{E_G \; due \; to \; PST} + \underbrace{\frac{Rn}{2}\{(A\theta + \eta\theta')^2 + Re\,\theta'^2\}}_{E_G \; due \; to \; Rn} + \underbrace{E_\Psi}_{E_G \; due \; to \; \Psi} , \tag{21}$$

$$E_{\Psi} = 2\frac{Br}{\xi}\left\{\left(f'+\frac{\eta}{2}f''\right)^2 + \left(g'+\frac{\eta}{2}g''\right)^2\right\} + \frac{Br}{2\xi}\left\{(f'+g')+\eta(f''+g'')\right\}^2 + \frac{Br}{\xi}\left\{(f'+g')+\frac{\eta}{2}(f''+g'')\right\}^2$$

$$+ \frac{Br}{8\,\mathrm{Re}}\frac{1}{\xi}\left\{\begin{array}{l}2\,\mathrm{Re}\,f''- \\ \left((f+g)+2\eta(f'+g')+\eta^2(f''+g'')^2\right)\end{array}\right\}^2 + \frac{Br}{8\,\mathrm{Re}}\frac{1}{\xi}\left\{\begin{array}{l}2\,\mathrm{Re}\,g''- \\ \left((f+g)+2\eta(f'+g')+\eta^2(f''+g'')^2\right)\end{array}\right\}^2.$$

(22)

Equation (22) clearly discloses the involvement of three diverse roots of entropy generation (i.e., entropy generation due to the PST (E_{PST}), thermal radiation (E_{Rn}) and viscous dissipation (E_{Ψ}).

3.2. For the case of PSHF

The dimensionless locally generated entropy (E_G) is defined in the following way:

$$E_G = \frac{S_{Gen}}{S_{gen}} = \underbrace{\frac{(1+\gamma\varphi)}{2}\{(B\varphi+\eta\varphi')^2 + Re\,\varphi'^2\}}_{E_G\ due\ to\ PST} + \underbrace{\frac{Rn}{2}\{(B\varphi+\eta\varphi')^2 + Re\,\varphi'^2\}}_{E_G\ due\ to\ Rn} + \underbrace{E_{\Psi}}_{E_G\ due\ to\ \Psi}.$$

(23)

In the above equations, Re is the local Reynolds number, Br is the Brinkman number, and ξ is the finite temperature difference.

$$Re = \frac{U_w}{\nu}L, \quad Br = \frac{\mu U_w^2}{k_\infty \Delta T}, \quad \xi = \frac{\Delta T}{T_\infty}, \quad \Delta T = T_0 e^{A\frac{(x+y)}{2L}}$$

(24)

To calculate the irreversibility distribution (for the PST and PSHF cases), the Bejan number (Be) is given as:

$$Be = \frac{E_{PST}}{E_{PST} + E_{Rn} + E_{\Psi}},$$

(25)

$$Be = \frac{E_{PSHF}}{E_{PSHF} + E_{Rn} + E_{\Psi}}.$$

(26)

4. Series solution

To establish the series solutions, we considered a very efficient technique, particularly, the HAM (see [31−33]). When (6), (7), (15) and (16) are subject to boundary conditions (8) and (9), the HAM is applied to obtain the corresponding analytical solutions (17). You may quickly and simply get at your initial guesses and the linear operator by doing the following:

$$f_0(\eta) = 1 - e^{-\eta}, \quad g_0(\eta) = \alpha(1 - e^{-\eta}), \quad \theta_0(\eta) = e^{-\eta}, \quad \varphi_0(\eta) = \frac{e^{-\eta}}{1+\gamma},$$

(27)

$$L_f(f) = f''' - f', \quad L_g(g) = g''' - g', \quad L_\theta(\theta) = \theta'' - \theta, \quad L_\varphi(\varphi) = \varphi'' - \varphi.$$

(28)

A MATHEMATICA code has been constructed for the defined problem in which we endorse $(\hbar_f, \; \hbar_g, \; \hbar_\theta \; \text{and} \; \hbar_\varphi)$ as the auxiliary parameters for the unknown function $(f, \; g, \; \theta \; \text{and} \; \varphi)$, which gives the convergence region. To find the admissible values of $(\hbar_f, \hbar_g, \hbar_\theta \; \text{and} \; \hbar_\varphi)$ and the so called $\hbar-$ curves were developed as displayed for the 15th order of approximation in Figures 2 and 3. These figures show that the admissible values are $-0.7 \leq \hbar_f \leq -0.2, \; -0.6 \leq \hbar_g \leq -0.2, \; -0.6 \leq \hbar_\theta \leq -0.2$ and $-0.8 \leq \hbar_\varphi \leq -0.1$. It is further noticed that the range of admissible values of $\hbar$ increases by increasing the order of approximations. Figures 2 and 3 depict the values of $(\hbar_f, \; \hbar_g, \; \hbar_\theta \; \text{and} \; \hbar_\varphi)$.
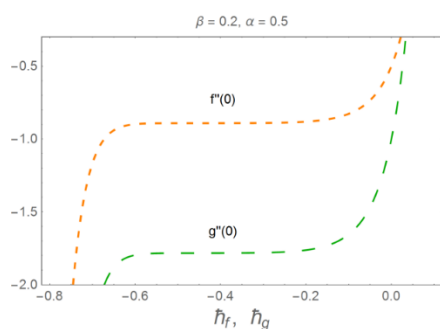
Figure 2. $\hbar$-curves for the functions $\hbar_f$ & $\hbar_g$.   **Figure 3.** $\hbar$-curves for the functions $\hbar_\theta$ & $\hbar_\varphi$.
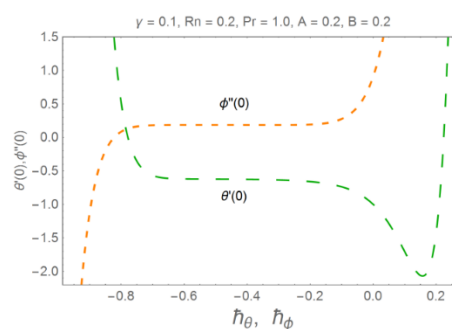
Table 1 gives knowledge about the approximation order, which helps us in making a judgment about the orders of approximations that is sufficient for the convergence. It is noticed that convergent solutions up to the fifth decimal place are acquired at just the 16th and 20th order of estimation.

Table 1: Approximations of different orders converge to the series solution when $\alpha = 0.5, \; \beta = 0.2, \; \gamma = 0.1, \; Rn = 0.2, \; Pr = 1.0, \; A = 0.2, \; B = 0.2, \; \hbar_f = \hbar_g = \hbar_\theta = \hbar_\varphi = -0.4$.

Order of approximation	$-f''(0)$	$-g''(0)$	$-\theta'(0)$	$\varphi''(0)$
1	1.44813	.72406	.87333	.51570
4	1.75472	.86584	.70194	.21325
8	1.78138	.88897	.64558	.18583
12	1.78208	.89124	.62985	.18581
16	1.78303	.89148	.62395	.18618
20	1.78303	.89148	.62135	.18634
30	1.78303	.89148	.62135	.18634
40	1.78303	.89148	.62135	.18634

5. Results and discussion

In this section, several graphical illustrations and numerical tables are presented to show the rheology of various parameters. Figures 4 and 5 were developed to visualize the behavior of the viscoelastic fluid parameter (Deborah number) on f and f', respectively. By analyzing these numbers, we conclude that raising the Deborah number slows down the flow of the fluid. Physically, $(\beta < 1)$ relates to fluids for which the relaxation time is less than the characteristic deformation time. This is the case for fluids with low viscosities. Thus, the non-Newtonian fluid behaves as a purely viscous fluid. On the other hand, when $(\beta < 1)$, the fluid behaves as if it were an elastically solid substance. Figures 6 and 7 visualize the response of the stretching ratio parameter on $g(\eta)$ and $g'(\eta)$, respectively. It is observed in these figures that the fluid velocity significantly increases with an enhancement in the stretching parameter. Physically, we can conclude that for $\alpha = 0$, the flow reduces to two-dimensional, whereas $\alpha > 0$ corresponds to three-dimensional flow as is evident from Figure 6. Moreover, it is also observed that the flow is axisymmetric when 1.0. Figure 8 demonstrates the consequences of temperature-dependent thermal conductivity. A significant increase in the fluid energy is observed when is increased. The thermal boundary layer thickness accelerates fruitfully when is increased. Figure 9 shows the impact of γ on φ. It is observed that as φ increases, the temperature of the fluid decreases.
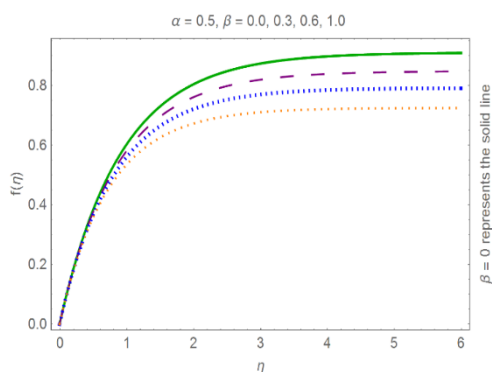
Figure 4. Influence of β on f.
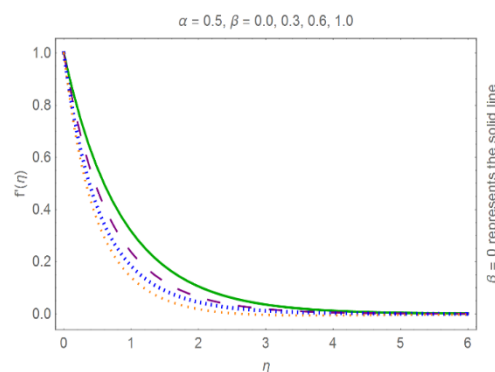
Figure 5. Influence of β on f'.
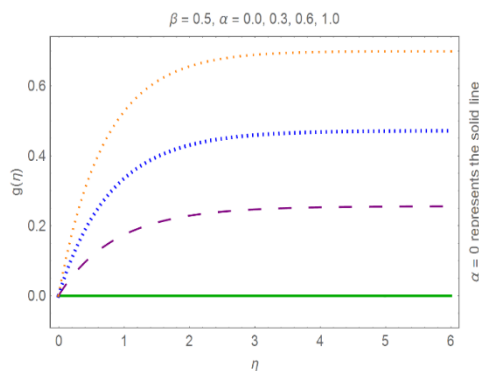
Figure 6. Influence of α on g.
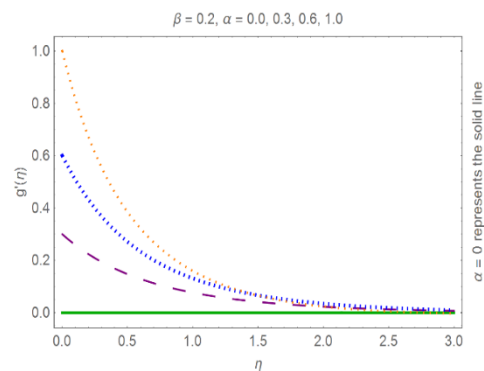
Figure 7. Influence of α on g'.
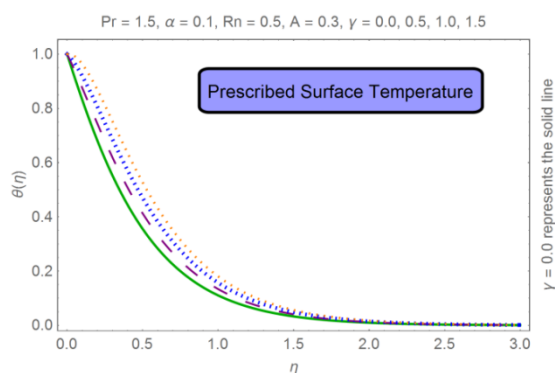
Figure 8. Influence of γ on θ for PST.
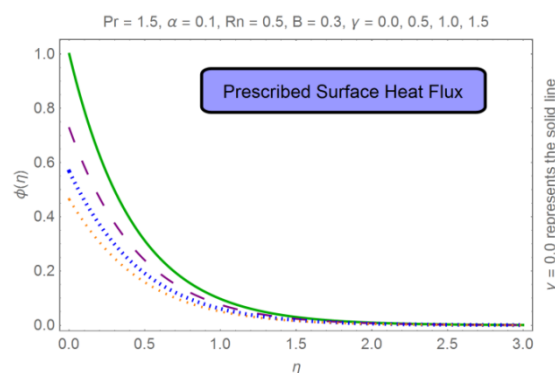
Figure 9. Influence of γ on ϕ for PSHF.

Figures 10 and 11 illustrate the different values of the radiation parameter *(Rn)* throughout time. It is perceived that, with the increase of radiation there is an increase in both temperature profiles (i.e., PST and PSHF), which is obvious. The influence of the stretching ratio parameter for (*Pr* = 0.7 and 0.02) on the temperature profile is plotted in Figures 12 and 13, respectively. The temperature fields (PST and PSHF) demonstrate purposeful overshoots for a low *Pr* (liquid metal = 0.02), whereas, for a high *Pr* (air=0.02) the temperature variation was not that crucial. From a physical perspective, we can conclude that the reaction of the stretching ratio parameter is very impressive in the case of liquid metals because of a low viscosity, whereas for higher *Pr* values, the overshoot does not exist because a high *Pr* indicates a more viscous fluid.
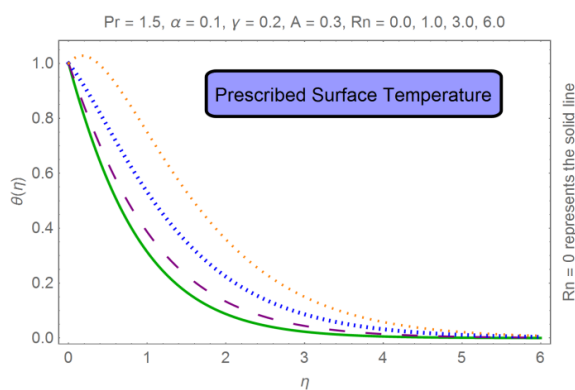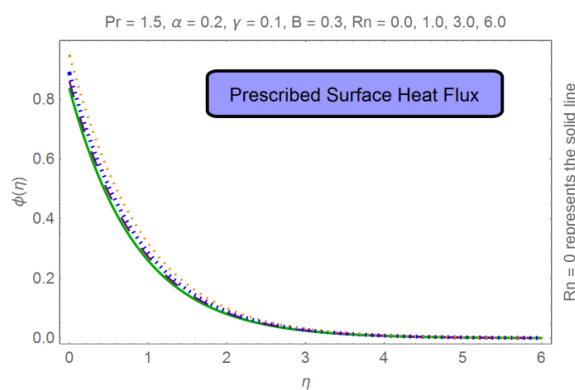

Figure 10. Influence of Rn on θ for PST.
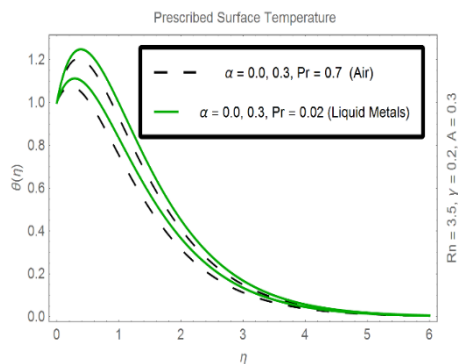
Figure 11. Influence of Rn on ϕ for PSHF.

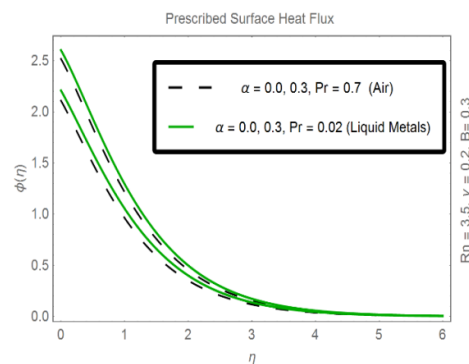**Figure 12.** Comparison of results: Air vs liquid metals on θ .

Figure 13. Comparison of results: Air vs liquid metals on ϕ .

Figures 14−19 were sketched to illustrate the behavior of the entropy generation (E_G) under the influence of various physical parameters, i.e., the Brinkman number (Br), Prandtl number (Pr) and thermal radiation (Rn) as function of the PST and PSHF wall conditions. Figures 14 and 15 show the influence of E_G with increasing values of Br for the PST and PSHF wall conditions, respectively. It can be seen that E_G is the increasing function of Br for both (PST and PSHF) situations. Physically, an increase in E_G is due to the fact that as Br increases, the fluid friction increases near the surface, which consequently increases the entropy of the system. The influence of increasing Pr on the entropy number is represented in Figure 16 (PST) and Figure 17 (PSHF). In these figures, we have plotted different ranges of Pr (i.e., liquid metal, air, sea water and engine oil). It can be seen that the entropy of the system is frequently increasing for increasing values of the Prandtl number. Impact of Rn is observed in Figures 18 and 19 as a function of the entropy generation for the PST and PSHF conditions, respectively. It is noticed that an increase in the radiation parameter leads to a decrease in the entropy production. Physically, an increase in Rn means a decrease in the buoyancy force, which subsequently decreases the entropy production.
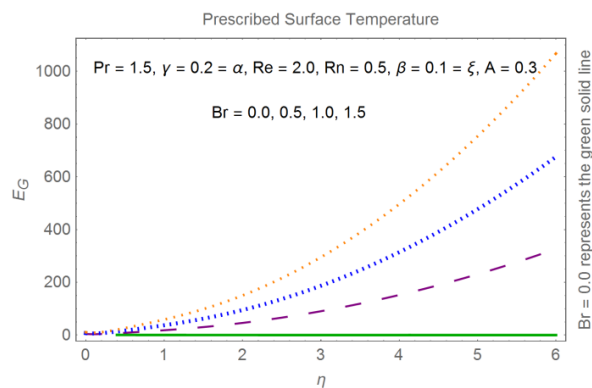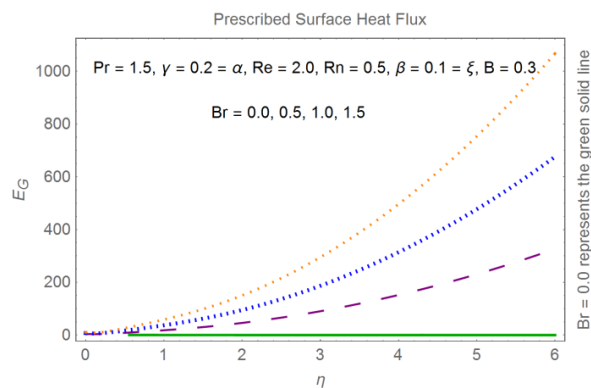

Figure 14. Influence of Br on E_G for PST.
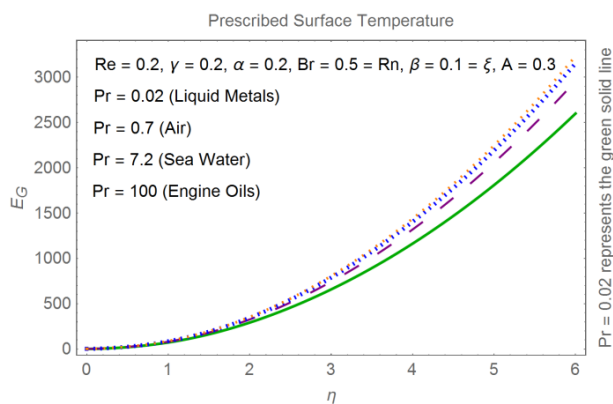

Figure 15. Influence of Br on E_G for PSHF.

Figure 16. Influence of Pr on E_G for PST.
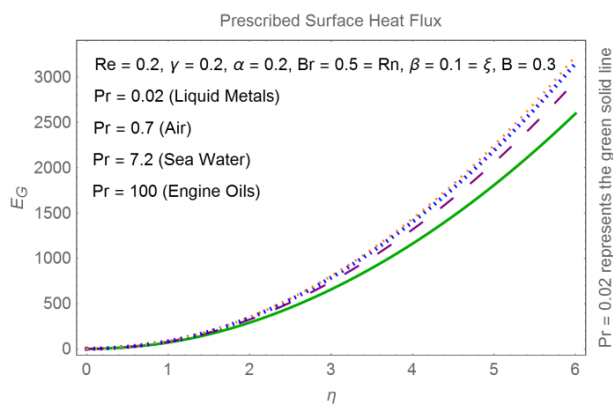
Figure 17. Influence of Pr on E_G for PSHF.
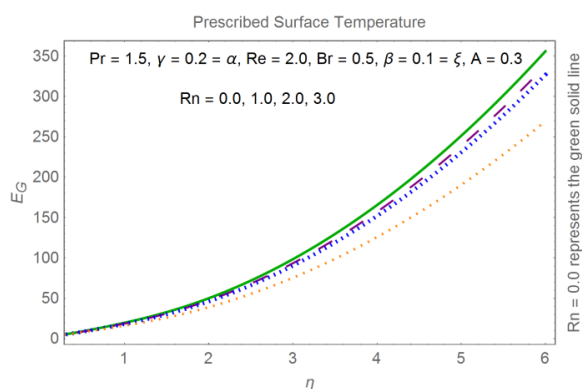

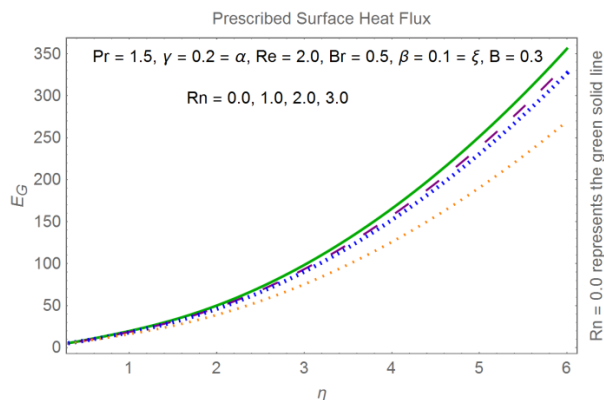**Figure 18.** Influence of Rn on E_G for PST.

Figure 19. Influence of Rn on E_G for PSHF.

Figures 20−23 illustrate the physical sense of the Bejan number (Be) for increasing values of the Brinkman number (Br) and radiation parameter (Rn). It is observed that Be continuously decreases with increasing values of $Br,$ which is due to the fact that heat transfer irreversibility is small as compared to the total irreversibility: see Figures 20 and 21. On the other hand, Be increases effectively with an enhancement in Rn for both the PST and PSHF wall conditions (see Figures 22 and 23).
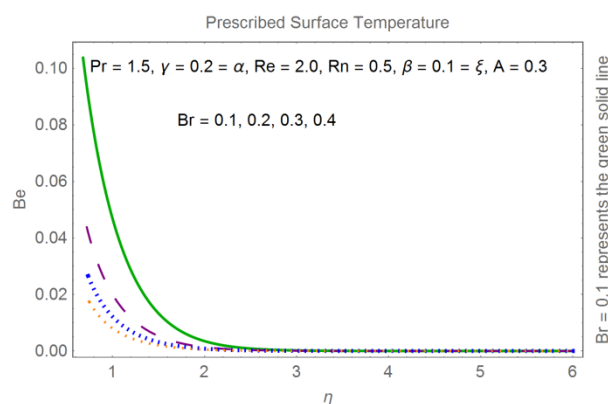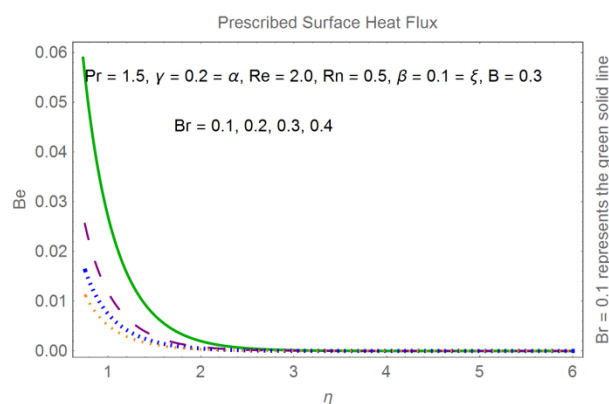
Figure 20. Influence of Br on Be for PST.

Figure 21. Influence of Br on Be for PSHF.
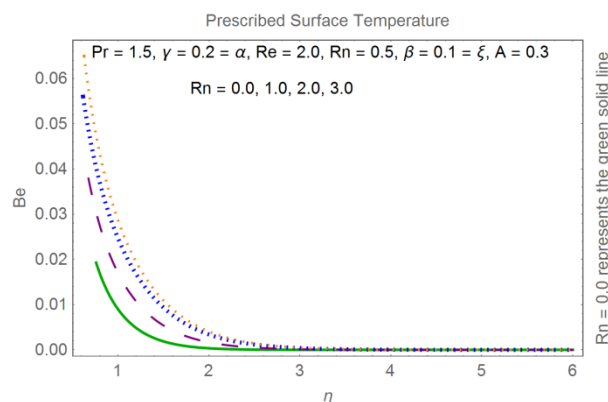
Figure 22. Influence of Rn on Be for PST.
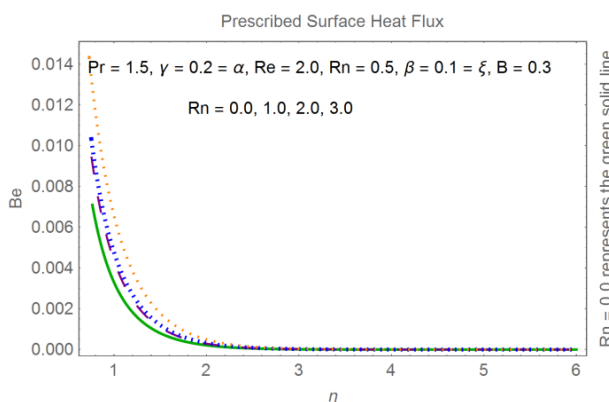
Figure 23. Influence of Rn on Be for PSHF.

Table 2 gives the comparison of velocity profiles. Consistency is found between the numerical and HAM results. Table 2 gives the numerical temperature dependent thermal conductivity for multiple values of α and Rn . Table 3 gives the numerical PST and PSHF wall conditions with respect to entropy for various values of the Brinkman number while other parameters remain fixed. It is noted that, as we increase the domain, i.e., $(\eta \rightarrow \infty)$, both wall conditions are becoming fully matured.

Table 2. Specific numerical values for the PST and PSHF for different values of η and $Pr = 1.5$, $\gamma = 0.1$, $A = 0.2$, $B = 0.2$.

Parameters		Prescribed Surface Temperature			Prescribed Surface Heat Flux		
α	Rn	$\eta = 0.0$	$\eta = 2.5$	$\eta = 5.0$	$\eta = 0.0$	$\eta = 2.5$	$\eta = 5.0$
0.0	5.0	1.00000	0.28385	0.03857	1.93112	0.34177	0.04194
2.5		1.00000	0.16762	0.01665	1.70385	0.21745	0.02048
5.0		1.00000	0.05138	-0.0052	1.47658	0.09312	-0.0009
0.2	0.0	1.00000	0.06934	0.00313	1.00385	0.07065	0.00347
	3.0	1.00000	0.19247	0.02334	1.54931	0.22736	0.02552
	6.0	1.00000	0.31559	0.04355	2.09476	0.38406	0.04757

Table 3. Numerical values for the PST and PSHF with respect to the entropy number for various values of η and $Pr = 1.5$, $\gamma = \alpha = 0.2$, $A = B = 0.2$, $\beta = \xi = 0.1$, $Re = 2.0$, $Rn = 0.5$.

Parameters	PST against E_G			PSHF against E_G		
Br	$\eta = 0.0$	$\eta = 3.0$	$\eta = 6.0$	$\eta = 0.0$	$\eta = 3.0$	$\eta = 6.0$
0.0	1.339784	0.040114	0.000239	1.221426	0.014548	0.000239
2.5	4.525782	55.59538	189.2253	4.436658	55.57690	189.2253
5.0	7.577889	114.6446	391.3971	7.516286	114.6324	391.3971
0.2	10.57192	181.2563	618.1717	10.53617	181.2496	618.1717

Figures 24 and 25 show the streamline behavior for two and three-dimensional Maxwell fluid models. It was found that the streamline for two and three-dimensional flows are quite interesting.
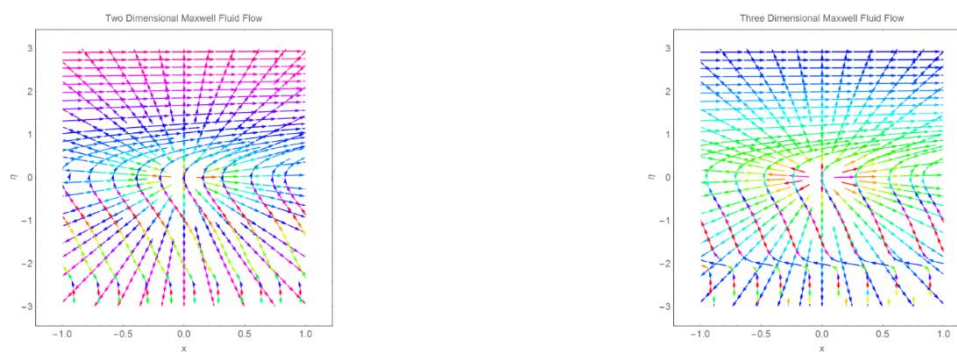
Figure 24. Stream lines for 2-D Maxwell fluid.   **Figure 25.** Stream lines for 3-D Maxwell fluid.

6. Conclusions

The main ideas of the analysis are as follows:
- The Deborah number retards the fluid velocity.
- Three-dimensional flow reduces to two-dimensional flow for $\alpha = 0$.
- The non-Newtonian fluid behaves as a purely viscous fluid when the Deborah number exceeds 1.
- Temperature-dependent thermal conductivity has quite different effects in the PST and PSHF cases.
- The stretching ratio parameter has a greater over shoot for liquid metals (low Prandtl number).
- It is noted from Table 3 that as the domain increases, the solution settles down for both PST and PSHF wall conditions.
- In the case of the Bejan number, the magnitude of the PSHF is greater than the PST.
- The Bejan number is directly proportional to the radiation parameter and inversely proportional to the Brinkman number.
- It is noted from Table 3 that, as the domain increases, the solution settles down for both the PST and PSHF wall conditions.

Acknowledgments

Conflict of interest

The authors declare that they have no competing interests.

References

1. A. Bejan, A study of entropy generation in fundamental convective heat transfer, *J. Heat Transfer*, **101** (1979), 718−725. https://doi.org/10.1115/1.3451063

2. M. M. Rashidi, A. B. Parsab, O. Anwar Beg, L. Shamekhib, S. M. Sadri, Tasveer A. Bég, Parametric analysis of entropy generation in magneto-hemodynamic flow in a semi-porous channel with OHAM and DTM, *Appl. Bionics Biomech.*, **11** (2014), 47−60. https://doi.org/10.3233/ABB-140086

3. Y. Aksoy, Effects of couple stresses on the heat transfer and entropy generation rates for a flow between parallel plates with constant heat flux, *Int. J. Therm. Sci.*, **107** (2016), 1−12. https://doi.org/10.1016/j.ijthermalsci.2016.03.017

4. M. N. Abrar, R. Ul Haq, M. Awais, I. Rashid, Entropy analysis in a cilia transport of nanofluid under the influence of magnetic field, *Nucl. Eng. Technol.*, **49** (2017) 1680−1688. https://doi.org/10.1016/j.net.2017.09.007

5. A. Kamran, S. Hussain, M. Sagheer, N. Akmal, A numerical study of magnetohydrodynamics flow in Casson nanofluid combined with Joule heating and slip boundary conditions, *Results phys.*, **7** (2017), 3037−3048. https://doi.org/10.1016/j.rinp.2017.08.004

6. M. U. Rashid, M. Mustafa, A study of heat transfer and entropy generation in von Karman flow of Reiner-Rivlin fluid due to a stretchable disk, *Ain Shams Eng. J.*, **12** (2021), 875−883. https://doi.org/10.1016/j.asej.2020.06.017

7. M. N. Abrar, M. Sagheer, S. Hussain, Entropy analysis of Hall current and thermal radiation influenced by cilia with single-and multi-walled carbon nanotubes, *Bull. Mater. Sci.*, **42** (2019), 250. https://doi.org/10.1007/s12034-019-1822-4

8. M. N. Abrar, M. Sagheer, S. Hussain, Entropy analysis of SWCNT & MWCNT flow induced by collecting beating of cilia with porous medium, *J. Cent. South Univ.*, **26** (2019), 2109−2118. https://doi.org/10.1007/s11771-019-4158-8

9. M. N. Abrar, M. Sagheer, S. Hussain, Entropy formation analysis for the peristaltic motion of ferrofluids in the presence of Joule heating and fluid friction phenomena in a plumb duct, *J. Nanofluids*, **8** (2019), 1305−1313. https://doi.org/10.1166/jon.2019.1672

10. M. N. Abrar, M. Sagheer, S. Hussain, Thermodynamics analysis of Joule heating and internal heat source over an inclined ciliated tube, *Physica A*, **549** (2020), 123983. https://doi.org/10.1016/j.physa.2019.123983

11. M. N. Abrar, M. Sagheer, S. Hussain, Entropy generation during peristaltically flowing nanofluid in an axisymmetric channel with flexible walls, *Phys. Scr.*, **95** (2020), 035206. https://doi.org/10.1088/1402-4896/ab4aab

12. B. C. Sakiadis, Boundary-layer behavior on continuous solid surfaces: I. Boundary-layer equations for two-dimensional and axisymmetric flow, *AIChE J.*, **7** (1961), 26−28. https://doi.org/10.1002/aic.690070108

13. A. J. Singh, Three-dimensional flow of a viscous fluid with heat and mass transfer, Int. *Commun. Heat Mass*, **32** (2005), 1420−1429. https://doi.org/10.1002/fld.2252

14. R. Razzaq, U. Farooq, J. Cui, T. Muhammad, Non-similar solution for magnetized flow of Maxwell nanofluid over an exponentially stretching surface, *Math. Probl. Eng.*, **2021** (2021), 5539542. https://doi.org/10.1155/2021/5539542

15. R. Razzaq, U. Farooq, Non-similar forced convection analysis of Oldroyd-B fluid flow over an exponentially stretching surface, *Adv. Mech. Eng.*, **13** (2021). https://doi.org/10.1177/16878140211034604

16. J. Cui, R. Razzaq, U. Farooq, W. A. Khan, F. B. Farooq, T. Muhammad, Impact of non-similar modeling for forced convection analysis of nano-fluid flow over stretching sheet with chemical reaction and heat generation, *Alex. Eng. J.*, **61** (2022), 4253−4261. https://doi.org/10.1016/j.aej.2021.09.045

17. U. Umer, R. Razzaq, M. I. Khan, Yu-M. Chu, D. C. Lu, Modeling and numerical computation of nonsimilar forced convective flow of viscous material towards an exponential surface, *Int. J. Mod. Phys. B*, **35** (2021), 2150118. https://doi.org/10.1142/S0217979221501186

18. U. Farooq, D. C. Lu, S. Ahmed, M. Ramzan, J. D. Chung, F. A. Chandio, Computational analysis for mixed convective flows of viscous fluids with nanoparticles, *J. Therm. Sci. Eng.*, **11** (2019), 021013. https://doi.org/10.1115/1.4043092

19. R, Talat, M. Mustafa, M. Asif Farooq, Modeling heat transfer in fluid flow near a decelerating rotating disk with variable fluid properties, *Int. Commun. Heat Mass*, 116 (2020), 104673. https://doi.org/10.1016/j.icheatmasstransfer.2020.104673

20. D. Qaiser, Z. Zheng, M. R. Khan, Numerical assessment of mixed convection flow of Walters-B nanofluid over a stretching surface with Newtonian heating and mass transfer, *Therm. Sci. Eng. Prog.*, **22** (2021), 100801. https://doi.org/10.1016/j.tsep.2020.100801

21. M. N. Khan, N. Ullah, J. Z. Khan, D. Qaiser, M. R. Khan, Analysis of Maxwell bioconvective nanofluids with surface suction and slip conditions in the presence of solar radiations, *J. Phys. Commun.*, **5** (2021), 115014. https://doi.org/10.1088/2399-6528/ac36b4

22. J. Cui, S. Munir, U. Farooq, M. E. A. Rabie, T. Muhammad, R. Razzaq, On numerical thermal transport analysis of three dimensional bioconvective nanofluid flow, *J. Math.*, **2021** (2021), 5931989. https://doi.org/10.1155/2021/5931989

23. J. Cui, S. Munir, S. F. Raies, U. Farooq, R. Razzaq, Non-similar aspects of heat generation in bioconvection from flat surface subjected to chemically reactive stagnation point flow of Oldroyd-B fluid, *Alex. Eng. J.*, **61** (2022), 5397−5411. https://doi.org/10.1016/j.aej.2021.10.056

24. J. Cui, M. Safeeer, U. Farooq, M. E. A. Rabie, T. Muhammad, Significance of non-similar modeling in the entropy analysis of chemically reactive magnetized flow of nanofluid subjected to thermal radiations and melting heat condition, *AIP Adv.*, 11 (2021), 085018. https://doi.org/10.1063/5.0058491

25. M. I. Khanb, S. Qayyum, Yu-M. Chu, N. B. Khan, S. Kadry, Transportation of Marangoni convection and irregular heat source in entropy optimized dissipative flow, *Int. Commun. Heat Mass*, **120** (2021), 105031. https://doi.org/10.1016/j.icheatmasstransfer.2020.105031

26. G, Bing, S. A. Khan, M. I. Khan, E. R. El-Zahar, M. Y. Malik, A. S. Alqahtani, et al., Entropy optimized analysis for the radiative flow of a nanofluid: the Darcy-Forchheimer model, *Wave Random Complex*, 2022. https://doi.org/10.1080/17455030.2022.2061082

27. A. Ali, K. Shehzadi, M. Sulaiman, S. Asghar, Heat and mass transfer analysis of 3D Maxwell nanofluid over an exponentially stretching surface, *Phys. Scripta*, **94** (2019), 065206. https://doi.org/10.1088/1402-4896/ab07cf

28. A. Ali, J. Akhtar, H. J. Anjum, M. Awais, Z. Shah, P. Kumam, 3D nanofluid flow over exponentially expanding surface of Oldroyd-B fluid, *Ain Shams Eng. J.*, **12** (2021), 3939−3946. https://doi.org/10.1016/j.asej.2021.01.026

29. S. Khattak, M. Ahmed, M. N. Abrar, S. Uddin, M. Sagheer, M. F. Javeed, Numerical simulation of Cattaneo-Christov heat flux model in a porous media past a stretching sheet, *Wave Random Complex*, 2022. https://doi.org/10.1080/17455030.2022.2030503

30. A. S. Khan, M. N. Abrar, S. Uddin, M. Awais, I. Usman, Entropy generation due to micro-rotating Casson's nanofluid flow over a nonlinear stretching plate: numerical treatment, *Wave Random Complex*, 2022. https://doi.org/10.1080/17455030.2022.2067376

31. T. Liu, Porosity reconstruction based on Biot elastic model of porous media by homotopy perturbation method, *Chaos Soliton Fract.*, **158** (2022), 112007. https://doi.org/10.1016/j.chaos.2022.112007

32. T. Liu, Parameter estimation with the multigrid-homotopy method for a nonlinear diffusion equation, *J. Comput. Appl. Math.*, **413** (2022), 114393. https://doi.org/10.1016/j.cam.2022.114393

33. M. Sajid, M. Awais, S. Nadeem, T. Hayat, The influence of slip condition on thin film flow of a fourth-grade fluid by the homotopy analysis method, *Comput. Math. Appl.*, **56** (2008), 2019−2026. https://doi.org/10.1016/j.camwa.2008.04.022